Stochastic modeling of decadal variability in ocean gyres

D. Kondrashov[1] and P. Berloff[2]

[1]Department of Atmospheric and Oceanic Sciences and Institute of Geophysics and Planetary Physics, University of California, Los Angeles, California, USA, [2]Department of Mathematics, Imperial College London, London, UK

Abstract Decadal large-scale low-frequency variability of the ocean circulation due to its nonlinear dynamics remains a big challenge for theoretical understanding and practical ocean modeling. This paper presents a novel fully data driven approach that addresses this challenge. Proposed is non-Markovian low-order methodology with stochastic closure and use of mode decomposition by multichannel Singular Spectrum Analysis. The multilayer stochastic linear model is obtained from the coarse-grained eddy-resolving ocean model solution, and with high accuracy it reproduces the main statistical properties of the decadal variability. The proposed methodology does not depend on the governing fluid dynamics equations and geometry of the problem, and it can be extended to other ocean models and ultimately to the real data.

1. Background

Midlatitude atmosphere and ocean possess not only significant interannual variability but also several large-scale variability modes on decadal and interdecadal timescales: North Atlantic Oscillation, Atlantic Multidecadal Oscillation, and Pacific Decadal Oscillation. Oceanic evidence of these modes is found in the sea surface temperature [*Hansen and Bezdek*, 1996], hydrography [*Qiu and Joyce*, 1992], and altimetry [*Qiu and Chen*, 2005], and it is mostly expressed in structural changes of the eastward jet extensions and the adjacent recirculation zones of the main western boundary currents, such as the Gulf Stream and Kuroshio. Physical origins of these large-scale low-frequency variability (LFV) modes remain unclear, and it is not even known to what extent these origins are intrinsic atmospheric, intrinsic oceanic, or coupled oceanic-atmospheric. One of the reasons, why coupled ocean-atmosphere comprehensive general circulation models (GCMs) cannot distinguish between these scenarios, is inability of their oceanic model components to simulate mesoscale eddies and their impact on the large-scale currents accurately and for a long time. On the other hand, seasonally forced, eddy-resolving ocean-only GCMs exhibit significant intrinsic LFV variability of mesoscale activity [*Penduff et al.*, 2011], intergyre heat transport [*Hall et al.*, 2004], sea level height [*Cabanes et al.*, 2006], western boundary currents [*Taguchi et al.*, 2007], and meridional overturning circulation [*Biastoch et al.*, 2008]. This suggests that not only significant part of the LFV is intrinsic to the ocean but also oceanic mesoscale eddies could play significant role in driving it.

Present theoretical understanding of the intrinsic LFV of the ocean starts from the null hypothesis that the ocean integrates high-frequency atmospheric forcing and responds in terms of the red variability spectrum [*Hasselman*, 1976]. However, over the last 20 years it became evident that in the presence of stochastic, seasonal, or constant atmospheric forcing, the most significant intrinsic LFV of the ocean is not red but operates on interannual-to-interdecadal time scales. One idea is that this variability can be understood in terms of early bifurcations of the forced and dissipative dynamical systems governing ocean circulation (e.g., review by *Dijkstra and Ghil* [2005]). In this approach, it is argued that the ocean variability is steered by the underlying, unstable low-dimensional attractors, and bifurcations of the attractors can be inspected by varying control parameters, such as the eddy diffusivity coefficients that parameterize effects of the mesoscale eddies. Other theoretical ideas for the LFV are excitation by external forcing of LFV basin modes linearized around the state of rest [*Cessi and Louazel*, 2001; *Huck and Vallis*, 2001], interaction of the deep western boundary current with the wind-driven gyres [*Katsman et al.*, 2001], instabilities of the thermohaline circulation [e.g., *Weaver et al.*, 1993], intermittent intrusions of potential vorticity that interrupt growth of the western boundary current recirculation zones [*Qiu and Miao*, 2000], eddy-topography coupling in the Southern Ocean [*Hogg and Blundell*, 2006], and mesoscale ocean-atmosphere coupling [*Hogg et al.*, 2009].

The understanding that oceanic eddies can collectively generate significant part of the climate variability came as a surprise, but it is already beginning to change our understanding of the global climate variability. Although it is recognized now that action of the oceanic mesoscale eddies is one of the main drivers of the midlatitude LFV (e.g., review by *Kwon et al.* [2010]), the involved eddy dynamics is poorly understood. Therefore, studying the LFV in *eddy-resolving* rather than eddy-parameterized models is of high priority. Recent joint analysis of the observations and comprehensive GCM solutions suggests that not only about half of the LFV in the ocean is intrinsic but also it is generated when significant fraction of mesoscale eddies is dynamically resolved rather than diffusively parameterized [*Penduff et al.*, 2011].

A very robust LFV mechanism, operating in a model of eddying, wind-driven oceanic gyres, has been discovered by *Berloff and McWilliams* [1999] and explained later by *Berloff et al.* [2007a]. This mechanism—referred to as the *Turbulent Oscillator* (TO)—is driven by competition between the eddy-induced flow rectification and the eddy-induced potential vorticity anomalies, and both of these processes require explicit dynamical representation of the eddies, because they cannot be approximated as simple diffusive processes. The TO mechanism involves several important physical ingredients: (a) nonlinear rectification of the eddies, (b) relation between the rectification and the eastward jet barrier permeability, (c) geometric wind effect, (d) large-scale effects of the eddy-driven potential vorticity anomalies, and (e) nonlinear adjustment of the gyres. Furthermore, it is argued that TO can substantially couple with the atmospheric circulation [*Hogg et al.*, 2006; *Berloff et al.*, 2007b].

Along with dynamical understanding of the intrinsic variability goes the practical need of modeling this variability statistically, with reduced mathematical models, in which essential effects of mesoscale eddies are optimally parameterized, and the solution is represented by a few LFV modes. Various methods of the reduction have been considered to derive low-order LFV models for climate applications, and stochastic-based closure schemes appear to be most promising [*Williams*, 2005; *Chekroun et al.*, 2011b]; see also *Franzke et al.* [2014] for recent comprehensive review of the subject. Theoretical asymptotic approaches are based on applying stochastic homogenization techniques to governing equations of geophysical turbulence [*Majda et al.*, 1999; *Gottwald and Melbourne*, 2013]. The resulting stochastic differential equations perform best in the limit of clear scale separation between the explicitly resolved *slow (large) scales* and the unresolved *fast (small) scales*. Theoretical low-order reduction procedure of the stochastic parameterizing manifolds for partial-differential equations, on the other hand, introduce memory effects and do not rely on scale separation. The advances in low-order modeling of the midlatitude atmosphere were made with asymptotic techniques [*Franzke and Majda*, 2006], dynamically based linear stochastic models [*DelSole*, 2004], pure statistical data-driven approaches [*Kravtsov et al.*, 2009; *Strounine et al.*, 2010], linear inverse modeling [*Winkler et al.*, 2001], and linear models with state-dependent noise [*Sardeshmukh and Sura*, 2009]. Whereas in the atmosphere clear scale separation implies nearly instantaneous adjustment of the small scales to the large ones, in the ocean this assumption is not valid, and it is more appropriate to account for delayed correlations between the large and small scales, i.e., *memory effects*. These effects make low-order modeling of the oceanic LFV more difficult.

Despite steady progress, developing accurate eddy parameterizations, especially for low-order models, remains a big challenge. Recently, linear stochastic parameterizations of nonlinear small-scales interactions were proposed [*Majda et al.*, 2010; *Grooms et al.*, 2015], while *Kang and Harlim* [2012] extended this parametrization by using autoregressive models. Another approach calibrates stochastic eddy parametrization by eddy-resolving solutions: *Berloff* [2005] used spatially correlated autoregressive stochastic process to represent transient eddy forcing, whereas *Porta Mana and Zanna* [2014] conditioned probability density function (pdf) of the stochastic forcing onto the coarse-grained model variables. We note that LFV in these models was not explored.

This paper deals with low-order modeling of the intrinsic oceanic LFV (see section 3.1) by novel non-Markovian linear stochastic model. Our approach is data driven and data adaptive, and here the low-order model is based on the eddy-resolving solution, although the ultimate goal is to base it on the real observations. Instead of projecting the LFV on the Fourier basis [*Kang and Harlim*, 2012], we project it on the principal components [*Preisendorfer*, 1988] obtained from the Singular Spectrum Analysis [*Ghil et al.*, 2002]; see section 2.2. Evolution of the corresponding modes is predicted by the linear, coupled system of stochastic differential equations via Multilayer Stochastic Modeling (MSM) framework [*Kondrashov et al.*, 2014], which generalizes existing multilevel, regression-based approaches (see sections 2.3 and 3.2). The

nonlinear feedback of small scales on the large-scale LFV is parameterized by the combination of multilayer interactions, time-lagged Singular Spectrum Analysis (SSA) basis, and stochastic forcing. The explicit multilayer structure of the low-order model illuminates dynamical interactions between different modes of the LFV.

2. Models and Methods

2.1. Midlatitude Ocean Model

In this study the LFV data comes from the classical eddy-resolving double-gyre ocean model [*Berloff*, 2015]. The flow dynamics is governed by the quasigeostrophic potential vorticity (QG PV) equations for three stacked isopycnal layers:

$$\frac{\partial q_1}{\partial t} + J(\psi_1, q_1) + \beta \frac{\partial \psi_1}{\partial x} = \frac{1}{\rho_1 H_1} W + \nu \nabla^4 \psi_1, \tag{1}$$

$$\frac{\partial q_2}{\partial t} t + J(\psi_2, q_2) + \beta \frac{\partial \psi_2}{\partial x} = \nu \nabla^4 \psi_2, \tag{2}$$

$$\frac{\partial q_3}{\partial t} + J(\psi_3, q_3) + \beta \frac{\partial \psi_3}{\partial x} = -\gamma \nabla^2 \psi_3 + \nu \nabla^4 \psi_3, \tag{3}$$

where the layer index starts from the top, $J(,)$ is the Jacobian operator, $\rho_1 = 10^3$ kg m^{-3} is the upper layer density, $\beta = 2 \times 10^{-11}$ m^{-1} s^{-1} is the planetary vorticity gradient, $\nu = 20$ m^2 s^{-1} is the eddy viscosity coefficient, and $\gamma = 4 \times 10^{-8}$ s^{-1} is the bottom friction parameter. The basin size is $2L = 3840$ km, so that $-L \leq x \leq L$ and $-L \leq y \leq L$. The isopycnal layer depths are $H_1 = 250$, $H_2 = 750$, and $H_3 = 3000$ m. The PV anomalies q_i and the velocity stream functions ψ_i are related as

$$q_1 = \nabla^2 \psi_1 + S_1 (\psi_2 - \psi_1), \tag{4}$$

$$q_2 = \nabla^2 \psi_2 + S_{21} (\psi_1 - \psi_2) + S_{22} (\psi_3 - \psi_2), \tag{5}$$

$$q_3 = \nabla^2 \psi_3 + S_3 (\psi_2 - \psi_3), \tag{6}$$

where the stratification parameters $S_1, S_{21}, S_{22},$ and S_3 are such that the first and second Rossby deformation radii are Rd$_1$ = 40 km and Rd$_2$ = 20.6 km, respectively. The flow is forced by the prescribed wind stress curl $W(x, y)$. The double-gyre Ekman pumping $W(x, y)$ is asymmetric in order to avoid artificial symmetrization of the gyres:

$$W(x, y) = -\frac{\pi \tau_0 A}{L} \sin \left[\frac{\pi (L + y)}{L + B x} \right], \qquad y \leq B x, \tag{7}$$

$$W(x, y) = +\frac{\pi \tau_0}{L A} \sin \left[\frac{\pi (y - B x)}{L - B x} \right], \qquad y > B x, \tag{8}$$

where the asymmetry parameter is $A = 0.9$, the nonzonal tilt parameter is $B = 0.2$, and the wind stress amplitude is $\tau_0 = 0.8$ N m^{-2}.

There are no-flow-through and partial-slip boundary conditions on the lateral walls, augmented by the integral mass conservation constraints. The model is solved by the high-resolution numerical algorithm described in *Karabasov et al.* [2009], on the uniform 513^2 grid with 7.5 km nominal resolution. The solution is saved every 10 days over 2740 years—this time interval is unprecedentedly long for an eddy-resolving ocean model, but our study requires this length for obtaining highly accurate statistics of the LFV. Each snapshot of the solution was coarse grained by a local running window averaging with 120 km width to 65^2 grid with 60 km spacing. We checked that the outcome is not sensitive to moderate variations of the running window width.

Note that although QG double-gyre dynamics offers classical and rewarding framework for mesoscale eddy effects on the large-scale circulation, it has inherent limitations in terms of assumed small Rossby number, beta-plane approximation, and fixed stratification. Therefore, our work should be viewed as a forerunner for more complete study of the problem, with a comprehensive primitive-equation general circulation model.

2.2. Singular Spectrum Analysis

SSA [*Vautard and Ghil*, 1989; *Vautard et al.*, 1992] is a temporal domain extension of the spatial empirical orthogonal function (S-EOF) decomposition by principal component analysis (PCA) [*Preisendorfer*, 1988]. A comprehensive review of SSA and its computational details is in *Ghil et al.* [2002], and in this study we will utilize multivariate form of SSA, known also as multichannel SSA (M-SSA), but we will refer to it simply as SSA from herewith for brevity. SSA is based on diagonalization of the time-lagged covariance matrix of multivariate time series; its eigenvectors, given by the spatiotemporal empirical orthogonal functions (ST-EOFs), are an optimal set of data-adaptive, narrowband modes for decomposing the LFV. SSA is particularly efficient for quasiperiodic variability with phase and amplitude modulations. Projection of the data on each ST-EOF yields the corresponding spatiotemporal principal component (ST-PC). The entire data or its components corresponding to trends, oscillatory modes, or high-frequency noise can be reconstructed by using specific linear combinations of ST-PCs and ST-EOFs. Since ST-PCs do not carry phase information within the SSA time window, they simulate only spectral content and amplitude of the LFV. On the other hand, LFV phase information is captured by the reconstructed SSA components in the least squares sense, and the signal is found by convoluting the corresponding ST-PCs and ST-EOFs [*Ghil et al.*, 2002].

SSA utilizes time-lagged information associated with inherent memory effects; therefore, it is particularly fit for the Earth system modeling. This was demonstrated by *Mukhin et al.* [2014] for predicting dynamical transitions in the coupled ocean-atmosphere model and by *Chen et al.* [2014] who developed nonlinear generalization of SSA for low-order modeling of the atmosphere. In this study (section 3) we use ST-PCs of SSA to construct a low-order model of the oceanic LFV.

2.3. Multilayer Data-Driven Closure Models

This paper contributes to the area of inverse modeling that simulates dynamical properties of a system, given its observed statistical properties [*Penland and Sardeshmukh*, 1995]. We construct a prognostic model for evolution of the large-scale (macroscopic) fields, which can be estimated from incomplete observations. The key steps are estimating interactions between the macroscopic variables, identifying the hidden variables representing the unobserved small-scale degrees of freedom, and modeling the cross interactions between the macroscopic and hidden variables.

In Empirical Model Reduction (EMR) approach [*Kondrashov et al.*, 2005; *Kravtsov et al.*, 2005, 2009, 2011; *Kondrashov et al.*, 2013] macroscopic interactions can be either quadratic or linear, and the hidden variables are arranged into a "matrioshka" (i.e., stacked system) of layers. Each additional layer includes a new hidden variable, which is less autocorrelated than the one included on the previous layer, until some small decorrelation threshold is reached. The unknown coefficients introduced on each layer are estimated by the multilevel regression techniques (see *Kravtsov et al.* [2009] for a comprehensive review of the EMR methodology).

Strounine et al. [2010] showed that EMR is particularly effective when (1) small scales are modulated by, as well as feedback on the large scales, and (2) there is no significant time scale separation between the small and large scales. In this paper memory effects, associated with cross interactions between the macroscopic and hidden variables, appear naturally, as convolution terms obtained by recursive integration of the matrioshka levels. This setup is reminiscent of the Mori-Zwanzig closure formalism in statistical mechanics [*Zwanzig*, 2001; *Chekroun et al.*, 2011a; *Franzke et al.*, 2014].

Recently, *Kondrashov et al.* [2014] introduced multilayer stochastic model (MSM) framework as both generalization and continuous time limit of existing multilevel, regression-based approaches, including EMR and other multilayer models [*Majda and Harlim*, 2013; *Harlim et al.*, 2014]. The multilayer structure of MSMs provides a natural Markov approximation to the generalized Langevin equation of the Mori-Zwanzig formalism [*Chorin et al.*, 2002]. Also, *Kondrashov et al.* [2014] derived conditions on the structure of the nonlinear cross interactions between the macroscopic and hidden variables that guarantee the existence of a global attractor. This existence ensures well posedness of a broad class of MSM applications that include nonpolynomial predictors and nonlinearities not preserving energy.

In this study we consider simplified linear EMR model given by the following set of $p + 1$ equations:

$$\mathbf{x}_{k+1} - \mathbf{x}_k = -\mathbf{A}\mathbf{x}_k \delta t + \mathbf{r}_k^{(0)} \delta t,$$

$$\mathbf{r}_{k+1}^{(m-1)} - \mathbf{r}_k^{(m-1)} = \mathbf{L}^{(m)} \left[(\mathbf{x}_k)^T, \left(\mathbf{r}_k^{(0)}\right)^T, \ldots, \left(\mathbf{r}_k^{(m-1)}\right)^T \right]^T \delta t + \mathbf{r}_k^{(m)} \delta t, \quad 1 \le m \le p, \tag{9}$$
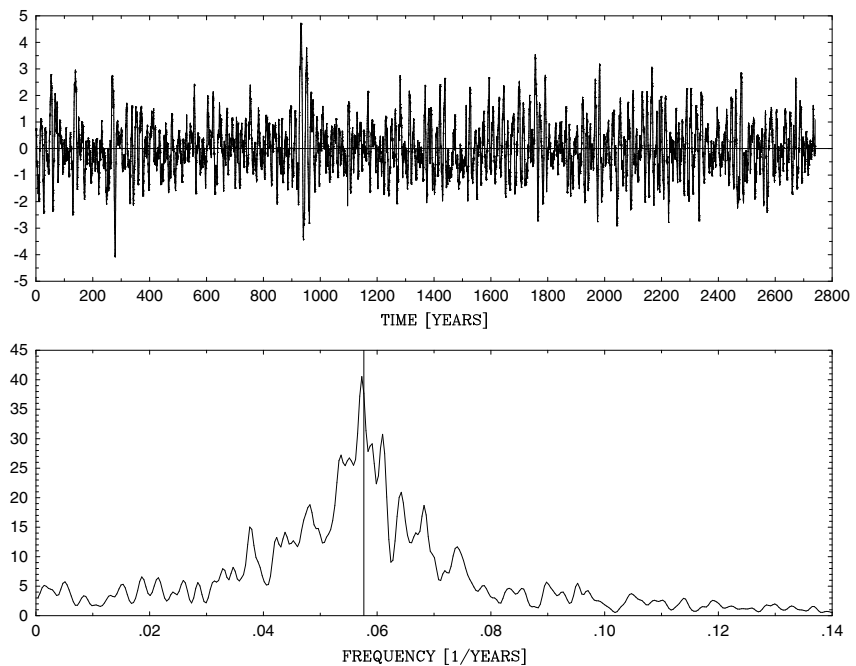
Figure 1. (top) Time series of the total energy from the ocean model reference solution and (bottom) its Fourier spectrum. The broadband decadal LFV has pronounced peak at ≈ 17 years. Only fluctuating part of the energy is shown in Figure 1 (top), and it is normalized by the standard deviation. The spectrum in Figure 1 (bottom) is normalized so that its integral is equal to unity.

where k is the discrete time index and $\mathbf{x}_k = \mathbf{x}(t_k)$ is the d-dimensional column vector $\mathbf{x}(t_k) := (x^1(t_k), \dots, x^d(t_k))^\mathsf{T}$ of the macroscopic variables predicted on the main level of the model. Matrix coefficients $\mathbf{A}$ represent linear dependencies of the macroscopic variables, and $\mathbf{r}_k^{(m-1)}$ is the vector of hidden variables predicted on the additional mth level of the model. Although more complex nonlinear cross interactions can be included [*Kondrashov et al.*, 2014], we consider only linear coupling of $\mathbf{r}_t^{(m-1)} \equiv r_k^{(m-1)}$ with variables $(\mathbf{x}, \mathbf{r}_t^{(0)}, \dots, \mathbf{r}_t^{(m-2)})$. Thus, the dynamics of hidden variables is given by the sequence of rectangular matrices $\mathbf{L}^{(m)}$ of increasing size. It is convenient to use a unit time step of $\delta t = 1$ in equation (9), see supporting information.

From the available time series of $\mathbf{x}$ and $\mathbf{r}_t^{(m-1)}$, the instantaneous tendencies $\delta \mathbf{x}/\delta t$ and $\delta \mathbf{r}_t^{(m-1)}/\delta t$ are found numerically by Euler time differencing, and then they are used to estimate the coefficients $\mathbf{A}$ and $\mathbf{L}^{(m)}$ by recursive least squares fits. The estimated residuals $\mathbf{r}_t^{(m)}$ are found recursively at the next $m+1$ level, until the recursive process stops at the pth level, when the estimated residual $\zeta_t \equiv \mathbf{r}_t^{(p)}$ has autocorrelation vanishing at the unit time lag. Then zero-lag covariance matrix of the residual converges to some constant matrix. The last residual is approximated as spatially correlated and temporally white noise $\mathbf{r}_t^{(p)} \approx \mathbf{\Sigma} \dot{\mathbf{W}}$, where $\dot{\mathbf{W}}$ denotes a d-dimensional Wiener process, and $\mathbf{\Sigma}$ is the Cholesky decomposition of its covariance matrix (see supporting information for more details of the recursive procedure and stopping criteria). This stochastic forcing is interpreted as nonlinear interactions of the smallest relevant scales.

3. Results and Discussion
### 3.1. LFV in Eddy-Resolving Ocean Model
The time mean of reference ocean model solution (see section 2.1) has the classical double-gyre structure (see Figure 1 of *Berloff et al.* [2007a]), and the ocean circulation is characterized by a robust large-scale decadal LFV, qualitatively similar to the turbulent oscillator studied by *Berloff et al.* [2007a]. The Fourier analysis of the solution's total energy time series shows that the LFV is spectrally broadband and dominated by a peak at ≈17 years (Figure 1). This variability is driven by transient mesoscale eddies [*Berloff et al.*, 2007a]. There is no clear scale separation between the eddies and large-scale flow, and the LFV accounts for relatively small fraction of the total variability, as demonstrated below by the detailed analysis.
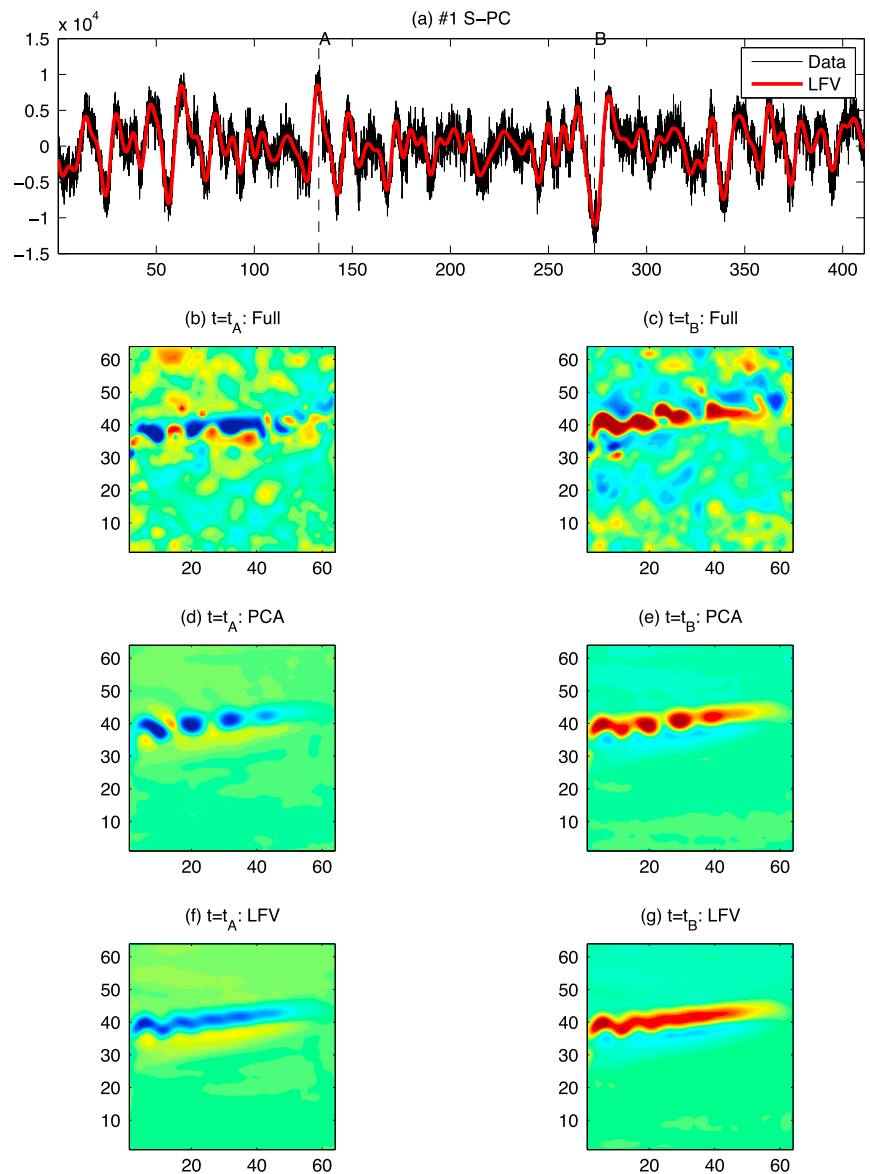
Figure 2. (a) Time series segment of a leading S-PC for an upper layer velocity stream function of QG model (black) and its pronounced decadal LFV component as captured by SSA reconstruction (red), see text for details; vertical dashed lines correspond to two energetic instances of SSA-LFV in opposite phase, $t = t_A$ and $t = t_B$, respectively. Spatial patterns of stream function at $t = t_A$ and $t = t_B$: (b, c) full anomalies, (d, e) PCA-filtered, and (f, g) decadal LFV by subsequent SSA filtration.

To systematically discern the LFV from the multitude of dynamically active scales, first, we compress the data by applying PCA to the time series of the upper ocean stream function anomaly, given by the record of 8×10^5 days sampled 10 days apart and coarse grained on 64×64 grid. Leading S-EOFs, selected from the total of 4096 modes, are retained for the subsequent SSA analysis. The leading $D = 6$ modes account for 6.1%, 5.6%, 5%, 3.8%, 3.3%, and 2.8% of the total variance, respectively ($\approx$27% altogether, see Figure S1 in the supporting information). The choice of $D = 6$ is motivated by the results of SSA discussed below.

The corresponding spatial principal components (S-PCs) are obtained by projecting the data on S-EOFs. The leading S-PC (Figure 2a) is dominated by highly intermittent decadal variability, but it also contains the small-amplitude, higher-frequency subannual variability. Next we apply SSA to the combined data set of retained S-PCs and to isolate oscillatory component of variability efficiently; the size of SSA time window M has to be longer than value of respective periodicity [*Ghil et al.*, 2002]. Here it suffices to choose
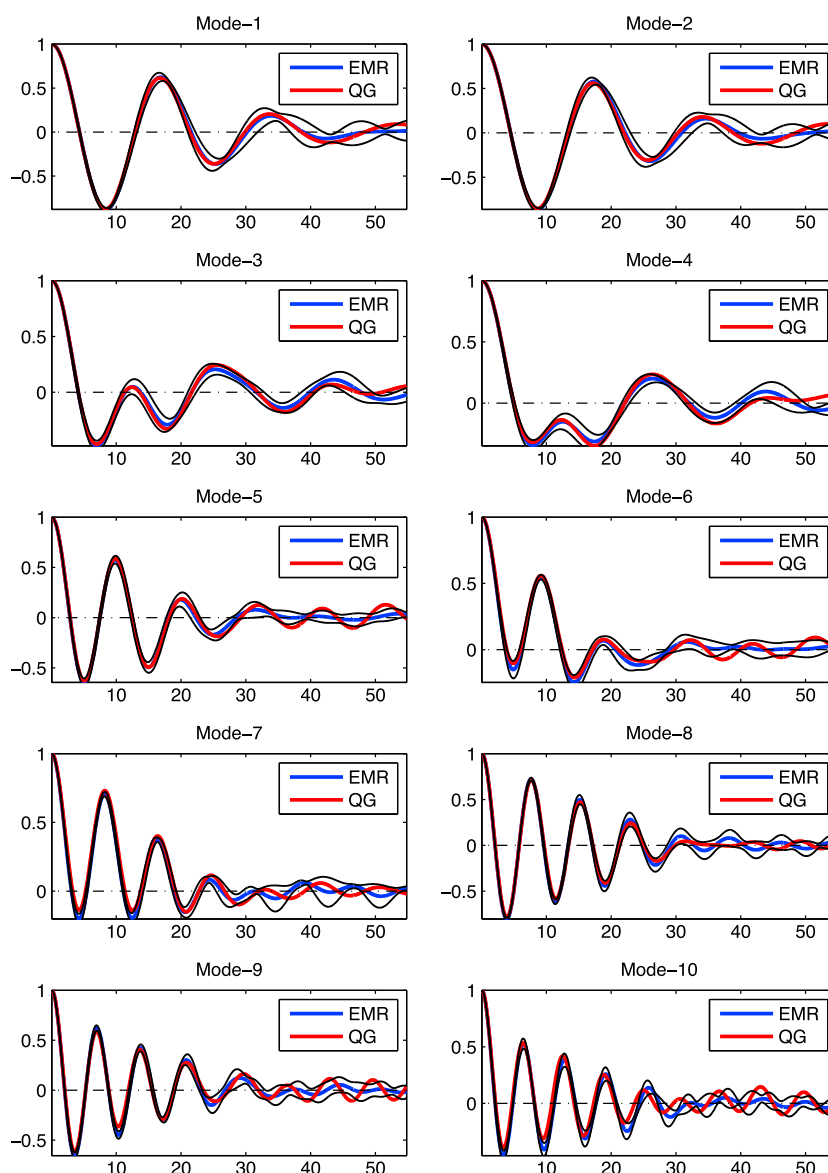
Figure 3. Autocorrelation functions (ACFs) of the 10 leading ST-PCs captured by SSA in an upper layer velocity stream function of QG model (see respective time series in Figure S3 in the supporting information): QG model solution = red, ensemble mean of the EMR-SSA random simulations = blue, standard deviation of the EMR-SSA ensemble = black, and x axis is in years. The EMR-SSA closure model captures well complex temporal modulations of decadal LFV. The first zero crossing of ACFs defines decorrelation time scales, shown in Figure S5 in the supporting information.

$M = 10^3$ samples (10^4 days $\approx$ 27 years) to extract LFV modes corresponding to broadband decadal peak (see Figure 1), and the reported results are robust to modest variation of M.

From the total of $DM = 6000$ ST-EOFs, we chose $d = 10$ leading modes (see Figures S1 and S2 in the supporting information) that capture 22% of the variance of the PCA-filtered field but focused on the first and sixth S-PC with 77% and 25% of the variance, respectively (this is equivalent to $\approx$6% of the total nonfiltered variance). More detailed SSA analysis showed that the higher-ranked S-PCs do not significantly contribute to the decadal LFV. The chosen time window ($M \approx 27$ years) and the SSA truncation level facilitated efficient extraction of the decadal LFV from the surrounding high-frequency subannual fluctuations (Figure 2a). Unlike *Berloff et al.* [2007a], we did not use temporal averaging prior to performing data-adaptive decomposition, and therefore, a relatively smaller fraction of variance is captured by decadal LFV in our results.
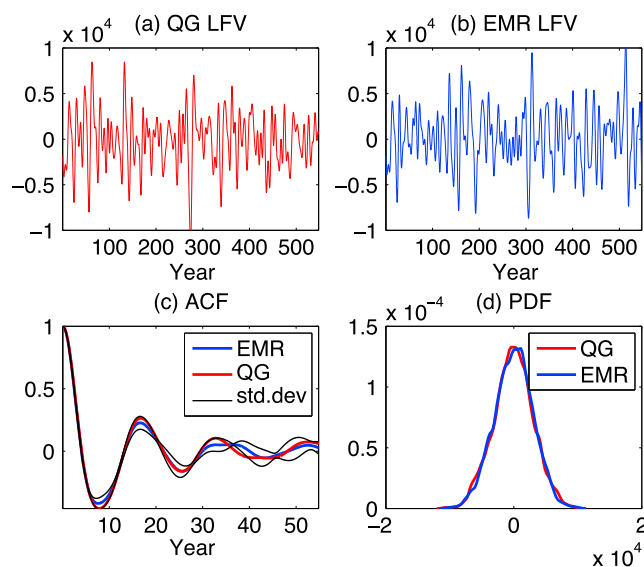
Figure 4. Statistics for decadal LFV of a leading S-PC: (a) short segment of time series for QG (same as in Figure 2a but longer); (b) stochastic realization by EMR-SSA; (c) ACF for QG of full-length time series ($8 \cdot 10^5$ days) = red, ensemble mean of the stochastic EMR-SSA realizations = blue, standard deviation of the EMR-SSA ensemble = black; and (d) 1-D-pdfs for QG (red) and EMR-SSA (blue).

Let us now discuss spatial patterns of different variability components. Figure 2 shows snapshots of the full and filtered upper ocean stream function anomalies at the two selected instances corresponding to the opposite phase in decadal LFV, $t = t_A$ and $t = t_B$, respectively. These patterns demonstrate that the LFV is dominated by coherent meridional shifts of the eastward jet extension separating the gyres (Figures 2f and 2g). Note that SSA filtered out the high-frequency, small-scale, and intensive meanders and eddies present in the PCA-filtered field (see Figures 2d and 2e).

Autocorrelation functions of the ST-PCs corresponding to the decadal LFV are characterized by the decaying oscillations (Figure 3) that result from the intermittency and sharp amplitude modulations of ST-PCs that are shown in Figure S3 in the supporting information, also see Figure 2a. Moreover, the characteristic decorrelation time scales, defined here as the lag corresponding to the first zero of the autocorrelation function, decrease with the rank and show no clear scale separation (see Figure S5 in the supporting information). In the next section we construct a data-driven MSM model that accurately reproduces these statistical features. Dynamical interactions of the decadal LFV with the variability represented by higher-rank ST-PCs account for the eddy effects associated with the ubiquitous planetary waves and with meanders of the eastward jet (see nonfiltered anomalies in Figures 2b and 2c). These interactions are effectively parameterized by the memory effects conveyed by the MSM framework.

3.2. MSM-SSA Model of the Decadal LFV
The low-order modeling and parameterization approaches, such as linear inverse modeling [*Penland and Sardeshmukh*, 1995] and EMR, are typically applied to a subset of the leading S-PCs obtained by PCA of the spatiotemporal field(s) of interest, e.g., **x** in equation (9). However, the corresponding data projection onto the leading S-EOFs has significant drawback: the resulting S-PCs capture only instantaneous spatial correlations, and the time-lagged correlations are not taken into account. Such correlations correspond to delayed feedbacks and external forcing effects that are more efficiently captured by SSA. This motivates the use of ST-PCs as macroscopic variables **x** in equation (9).

For understanding our results, it is useful to consider the most simple EMR application, in which the flow is harmonic in both space and time. SSA decomposes this field into the pair of eigenmodes with equal eigenvalues. The corresponding ST-PCs are harmonic in time, and they are in phase-quadrature relationship, i.e., one time series is time derivative of the other (e.g., *sine* and *cosine*). Application of the linear formulation of equation (9) to either ST-PC from this pair results in optimal EMR model with $p = 1$ and zero regression residual on the last level. Thus, only one additional level is needed for the *optimal* system of two equations describing the harmonic oscillator. This simple example suggests that for more complex dynamics, in which flow field is described by many spectrally mixed ST-PCs, additional levels of equation (9) are needed to simulate the observed statistics.

We found that the linear and unforced EMR model with large number of levels $p = 20$ successfully reproduces autocorrelation functions of dynamically modeled ST-PCs in QG reference solution (see Figure 3 and also Figure S3 in the supporting information). The decadal LFV corresponding to the leading S-PC of QG is simulated equally well, and the highly intermittent and sharp temporal modulations of the energetic
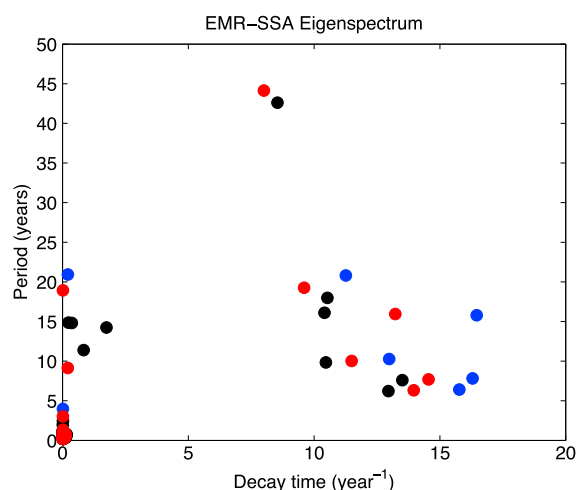
Figure 5. Eigenspectrum of multilevel linear operator EMR-SSA model for different numbers of levels p in equation (9): blue, $p = 10$; red, $p = 15$; and black, $p = 20$. The spectrum of the model's variability is determined by a few least damped modes with characteristic periods and decay rates in the decadal range that are excited by the stochastic forcing.

events in the EMR-SSA model are qualitatively similar to those in the original data (compare Figures 4a and 4b). Respective autocorrelation functions (Figure 4c) agree very well, ensuring excellent agreement for power spectrum due to Wiener-Khinchin theorem (not shown); probability density estimates based on a normal kernel function (Figure 4d) also match. The optimal number of the model levels is chosen according to the stopping criterion, see discussion of Figure S4 in the supporting information for details. Increasing the number of levels beyond optimal $p = 20$ does not bring further improvement in statistical match and only makes the low-order model computationally more expensive.

The complex dynamics of the EMR-SSA model results from cross interactions of the macroscopic, hidden **r** variables, and the stochastic forcing. In addition to linear self-interaction, the effective dynamics of macroscopic ST-PCs is also governed by the memory effects contributed by the hidden variables, as well as by red-noise stochastic forcing resulting from the propagation of a last level Wiener process through the successive linear levels of the model [*Kondrashov et al.*, 2014].

This dynamics can be further understood by the eigenmode analysis of the multilevel linear operator of the EMR-SSA model. This grand matrix has a block structure with its lower part formed by matrices **A** and $\mathbf{L}^{(m)}$, and the upper part formed by identity blocks corresponding to the forcings by $\mathbf{r}_t^{(m)}$ at the mth level (see equation (9) and assuming $\delta t = 1$). The eigenspectrum of the grand matrix is shown in Figure 5 for different numbers of levels p, and each complex eigenvalue represents damped oscillation with the decay rate and temporal period given by its real and imaginary part, respectively. Almost all eigenmodes are strongly damped, but about five oscillatory eigenmodes with decay times of 10–15 years and periods 5–20 years always exist. Superposition of these modes determines the LFV in the EMR.

The main benefit of using the SSA basis is that the memory effects inferred by the linear and multilayer interactions suffice for optimal closure of the low-order model, even though the real, fluid-dynamical mechanism of the intrinsic oceanic LFV is highly nonlinear [*Berloff et al.*, 2007a].

4. Conclusions

This paper deals with inverse modeling of the intrinsic oceanic LFV in the quasigeostrophic, wind-driven ocean gyres (see section 2.1) by novel non-Markovian and linear low-order model with stochastic closure (see section 2.3). The proposed approach is data driven and data adaptive, and the low-order model is derived from the coarse-grained eddy-resolving ocean model solution (see section 3.1). The resulting low-order multilayer stochastic model reproduces with high fidelity on the main statistical properties of the observed LFV, such as the autocorrelations and probability density distributions (see section 3.2).

Given small computational cost of the low-order model, there can be several important practical applications of our results. First, such models can be incorporated into oceanic components of climate system models, for analysis of the oceanic LFV feedbacks on the atmosphere. Second, such models can be used for understanding nonlinear interactions between different modes of the LFV. Third, dynamical analysis of low-order LFV models (cf. its eigenspectrum shown in Figure 5) can facilitate dynamical understanding of much more complex, high-dimensional oceanic models.

Since our approach does not depend on the governing fluid dynamics equations and geometry of the problem, it can be extended to other ocean models and ultimately to the real data. Further modifications in the inverse algorithm to obtain optimal closure are possible by including nonlinear cross interactions

between macroscopic and hidden variables [*Kondrashov et al.*, 2014], by using alternative data-adaptive decomposition to extract LFV, as well as extending the closure model to include spatiotemporal modes of faster and smaller scales.

References

Berloff, P. (2005), Random-forcing model of the mesoscale oceanic eddies, *J. Fluid Mech.*, *529*, 71–95.

Berloff, P. (2015), Dynamically consistent parameterization of mesoscale eddies. Part I: Simple model, *Ocean Modell.*, *87*, 1–19, doi:10.1016/j.ocemod.2014.12.008.

Berloff, P., and J. McWilliams (1999), Large-scale, low-frequency variability in wind-driven ocean gyres, *J. Phys. Oceanogr.*, *29*, 1925–1949.

Berloff, P., A. M. C. Hogg, and W. Dewar (2007a), The turbulent oscillator: A mechanism of low-frequency variability of the wind-driven ocean gyres, *J. Phys. Oceanogr.*, *37*(9), 2363–2386.

Berloff, P., S. Kravtsov, W. Dewar, and J. McWilliams (2007b), Ocean eddy dynamics in a coupled ocean-atmosphere model, *J. Phys. Oceanogr.*, *37*, 1103–1121.

Biastoch, A., C. Boning, and J. Lutjeharms (2008), Agulhas leakage dynamics affects decadal variability in Atlantic overturning circulation, *Nature*, *456*, 489–492.

Cabanes, C., T. Huck, and A. Colin de Verdiere (2006), Contributions of wind forcing and surface heating to interannual sea level variations in the Atlantic Ocean, *J. Phys. Oceanogr.*, *36*, 1739–1750.

Cessi, P., and S. Louazel (2001), Decadal oceanic response to stochastic wind forcing, *J. Phys. Oceanogr.*, *31*, 3020–3029.

Chekroun, M., D. Kondrashov, and M. Ghil (2011a), Predicting stochastic systems by noise sampling, and application to the El Niño-Southern Oscillation, *Proc. Natl. Acad. Sci. U.S.A.*, *108*(29), 11,766–11,771, doi:10.1073/pnas.101575.

Chekroun, M. D., E. Simonnet, and M. Ghil (2011b), Stochastic climate dynamics: Random attractors and time-dependent invariant measures, *Physica D*, *240*(21), 1685–1700.

Chen, N., A. J. Majda, and D. Giannakis (2014), Predicting the cloud patterns of the Madden-Julian Oscillation through a low-order nonlinear stochastic model, *Geophys. Res. Lett.*, *41*, 5612–5619, doi:10.1002/2014GL060876.

Chorin, A. J., O. H. Hald, and R. Kupferman (2002), Optimal prediction with memory, *Physica D*, *166*, 239–257.

DelSole, T. (2004), Stochastic models of quasigeostrophic turbulence, *Surv. Geophys.*, *25*, 107–149.

Dijkstra, H., and M. Ghil (2005), Low frequency variability of the large-scale ocean circulation: A dynamical systems approach, *Rev. Geophys.*, *43*, RG3002, doi:10.1029/2002RG000122.

Franzke, C., and A. J. Majda (2006), Low-order stochastic mode reduction for a prototype atmospheric GCM, *J. Atmos. Sci.*, *63*, 457–479.

Franzke, C. L., T. J. O'Kane, J. Berner, P. D. Williams, and V. Lucarini (2014), Stochastic climate theory and modeling, *Wiley Interdiscip. Rev. Clim. Change*, *6*, 63–78, doi:10.1002/wcc.3181111.

Ghil, M., et al. (2002), Advanced spectral methods for climatic time series, *40*, 1-1–1-41, doi:10.1029/2001RG000092.

Gottwald, G. A., and I. Melbourne (2013), Homogenization for deterministic maps and multiplicative noise, *Proc. R. Soc. London, Ser. A*, *469*(2156), 20130201.

Grooms, I., A. J. Majda, and K. Smith (2015), Stochastic superparameterization in a quasigeostrophic model of the Antarctic Circumpolar Current, *Ocean Modell.*, *85*, 1–15.

Hall, N., B. Barnier, T. Penduff, and J.-M. Molines (2004), Interannual variation of Gulf Stream heat transport in a high resolution model forced by reanalysis data, *Clim. Dyn.*, *23*, 341–351.

Hansen, D., and H. Bezdek (1996), On the nature of decadal anomalies in North Atlantic sea surface temperature, *J. Geophys. Res.*, *101*, 8749–8758.

Harlim, J., A. Mahdi, and A. Majda (2014), An ensemble kalman filter for statistical estimation of physics constrained nonlinear regression models, *J. Comput. Phys.*, *257*, 782–812.

Hasselman, K. (1976), Stochastic climate models. Part I: Theory, *Tellus*, *28*, 289–305.

Hogg, A., and J. Blundell (2006), Interdecadal variability of the Southern Ocean, *J. Phys. Oceanogr.*, *36*, 1626–1645.

Hogg, A., W. Dewar, P. Killworth, and J. Blundell (2006), Decadal variability of the midlatitude climate system driven by the ocean circulation, *J. Clim.*, *19*, 1149–1166.

Hogg, A., W. Dewar, P. Berloff, S. Kravtsov, and D. Hutchinson (2009), The effects of mesoscale ocean-atmosphere coupling on the large-scale ocean circulation, *J. Clim.*, *22*, 4066–4082.

Huck, T., and G. K. Vallis (2001), Linear stability analysis of the three-dimensional thermally-driven ocean circulation: Application to interdecadal oscillations, *Tellus*, *53A*, 526–545.

Kang, E., and J. Harlim (2012), Filtering nonlinear spatio-temporal chaos with autoregressive linear stochastic models, *Physica D*, *241*, 1099–1133.

Karabasov, S., P. Berloff, and V. Goloviznin (2009), CABARET in the ocean gyres, *Ocean Modell.*, *30*, 155–168.

Katsman, C., S. Drijfhout, and H. Dijkstra (2001), The interaction of a deep western boundary current and the wind-driven gyres as a cause for low-frequency variability, *J. Phys. Oceanogr.*, *31*, 2321–2339.

Kondrashov, D., S. Kravtsov, A. W. Robertson, and M. Ghil (2005), A hierarchy of data-based ENSO models, *J. Clim.*, *18*, 4425–4444.

Kondrashov, D., M. D. Chekroun, A. W. Robertson, and M. Ghil (2013), Low-order stochastic model and "past-noise forecasting" of the Madden-Julian oscillation, *Geophys. Res. Lett.*, *40*, 5305–5310, doi:10.1002/grl.50991.

Kondrashov, D., M. D. Chekroun, and M. Ghil (2014), Data-driven non-Markovian closure models, *Physica D*, *297*, 33–55, doi:10.1016/j.physd.2014.12.005.

Kravtsov, S., D. Kondrashov, and M. Ghil (2005), Multilevel regression modeling of nonlinear processes: Derivation and applications to climatic variability, *J. Clim.*, *18*, 4404–4424.

Kravtsov, S., D. Kondrashov, and M. Ghil (2009), Empirical model reduction and the modeling hierarchy in climate dynamics, in *Stochastic Physics and Climate Modeling*, edited by T. N. Palmer, and P. Williams, pp. 35–72, Cambridge Univ. Press, New York.

Kravtsov, S., D. Kondrashov, I. Kamenkovich, and M. Ghil (2011), An empirical stochastic model of sea-surface temperatures and surface winds over the Southern Ocean, *Ocean Sci.*, *7*(6), 755–770.

Kwon, Y.-O., M. Alexander, N. Bond, C. Frankignoul, H. Nakamura, B. Qiu, and L. Thompson (2010), Role of the Gulf Stream and Kurosio-Oyashio systems in large-scale atmosphere-ocean interaction: A review, *J. Clim.*, *23*, 3249–3281.

Majda, A. J., and J. Harlim (2013), Physics constrained nonlinear regression models for time series, *Nonlinearity*, *26*(1), 201–217.

Majda, A. J., I. Timofeyev, and E. Vanden-Eijnden (1999), Models for stochastic climate prediction, *Proc. Natl. Acad. Sci. U.S.A.*, *96*, 14,687–14,691.

Majda, A. J., J. Harlim, and B. Gershgorin (2010), Mathematical strategies for filtering turbulent dynamical systems, *Discrete Continuous Dyn. Syst.*, *27*(2), 441–486.

Mukhin, D., D. Kondrashov, E. Loskutov, A. Gavrilov, A. Feigin, and M. Ghil (2014), Predicting critical transitions in ENSO models, Part II: Spatially dependent models, *J. Clim.*, doi:10.1175/JCLI-D-14-00239.1.

Penduff, T., M. Juza, B. Barnier, J. Zika, W. Dewar, A.-M. Treguier, J.-M. Molines, and N. Audiffren (2011), Sea-level expression of intrinsic and forced ocean variabilities at interannual time scales, *J. Clim.*, *24*, 5652–5670.

Penland, C., and P. D. Sardeshmukh (1995), The optimal growth of tropical sea surface temperature anomalies, *J. Clim.*, *8*, 1999–2024.

Porta Mana, P., and L. Zanna (2014), Toward a stochastic parameterization of ocean mesoscale eddies, *Ocean Modell.*, *79*, 1–20.

Preisendorfer, R. W. (1988), *Principal Component Analysis in Meteorology and Oceanography*, 425 pp., Elsevier Sci., New York.

Qiu, B., and S. Chen (2005), Variability of the Kuroshio extension jet, recirculation gyre, and mesoscale eddies on decadal time scales, *J. Phys. Oceanogr.*, *35*, 2090–2103.

Qiu, B., and T. Joyce (1992), Interannual variability in the mid- and low-latitude western North Pacific, *J. Phys. Oceanogr.*, *22*, 1062–1079.

Qiu, B., and W. Miao (2000), Kuroshio path variations south of Japan: Bimodality as a self-sustained internal oscillation, *J. Phys. Oceanogr.*, *30*, 2124–2137.

Sardeshmukh, P., and P. Sura (2009), Reconciling non-Gaussian climate statistics with linear dynamics, *J. Clim.*, *22*, 1193–1207.

Strounine, K., S. Kravtsov, D. Kondrashov, and M. Ghil (2010), Reduced models of atmospheric low-frequency variability: Parameter estimation and comparative performance, *Physica D*, *239*, 145–166.

Taguchi, B., S. P. Xie, N. Schneider, M. Nonaka, H. Sasaki, and Y. Sasai (2007), Decadal variability of the Kuroshio Extension: Observations and an eddy-resolving model hindcast, *J. Clim.*, *20*(11), 2357–2377.

Vautard, R., and M. Ghil (1989), Singular spectrum analysis in nonlinear dynamics, with applications to paleoclimatic time series, *Physica D*, *35*, 395–424.

Vautard, R., P. Yiou, and M. Ghil (1992), Singular-spectrum analysis: A toolkit for short, noisy chaotic signals, *Physica D*, *38*, 95–126.

Weaver, A., J. Marotzke, P. Cummins, and E. Sarachik (1993), Stability and variability of the thermohaline circulation, *J. Phys. Oceanogr.*, *23*, 39–60.

Williams, P. D. (2005), Modelling climate change: The role of unresolved processes, *Philos. Trans. R. Soc. London, Ser. A*, *363*(1837), 2931–2946.

Winkler, C. R., M. Newman, and P. D. Sardeshmukh (2001), A linear model of wintertime low-frequency variability. Part I: Formulation and forecast skill, *J. Clim.*, *14*, 4474–4494.

Zwanzig, R. (2001), *Nonequilibrium Statistical Mechanics*, Oxford Univ. Press, New York.